DOPANT PROFILES WITH GRAZING INCIDENCE X-RAY DIFFRACTION

by

Mark Smith

A senior thesis submitted to the faculty of

Brigham Young University - Idaho

in partial fulfillment of the requirements for the degree of

Bachelor of Science

Department of Physics

Brigham Young University - Idaho

April 2026

BRIGHAM YOUNG UNIVERSITY - IDAHO

DEPARTMENT APPROVAL

of a senior thesis submitted by

Mark Smith

This thesis has been reviewed by the research advisor, research coordinator, and department chair and has been found to be satisfactory.

Date	David Oliphant, Advisor
Date	Jon Johnson, Committee Member
Date	Todd Lines, Committee Member
Date	Todd Lines, Thesis Coordinator
Date	Evan Hansen, Department Chair

ABSTRACT

DOPANT PROFILES WITH GRAZING INCIDENCE X-RAY DIFFRACTION

Mark Smith

Department of Physics

Bachelor of Science

In this work, grazing incidence X-ray diffraction (GIXRD) is utilized to investigate the depth profile of dopants in silicon. By systematically varying the X-ray incidence angle, one can precisely control the depth penetrated into doped silicon samples. This approach enables a non-destructive analysis of how dopant concentration evolves with depth. The findings provide crucial insights into the distribution and behavior of dopants, which is essential for optimizing semiconductor device performance and fabrication processes.

ACKNOWLEDGMENTS

Tylyn Smith for her patience in supporting me. Tyler Smith for encouraging me to study physics in university. Brother David Oliphant for his helpful guidance throughout my time spent learning here at BYUI. Brother Jon Johnson for his helpful introduction to solid state physics and computational methods. Lastly, Brother Todd Lines's enduring life and academic advice.

Contents

List of Figures

Chapter 1

Background

Solids can be divided into two broad types: crystalline, and amorphous. Crystalline solids have repeating structures that are predictable and consistent, exhibiting long-range order in the solid (figure 1.1). Amorphous solids have no repeating structures, and have no preferred orientation (figure 1.2).

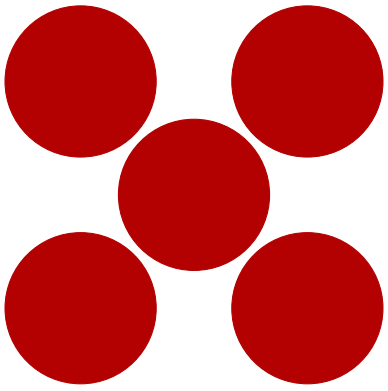

Figure 1.1 Arrangement of atoms in a crystalline face centered cubic (FCC) lattice

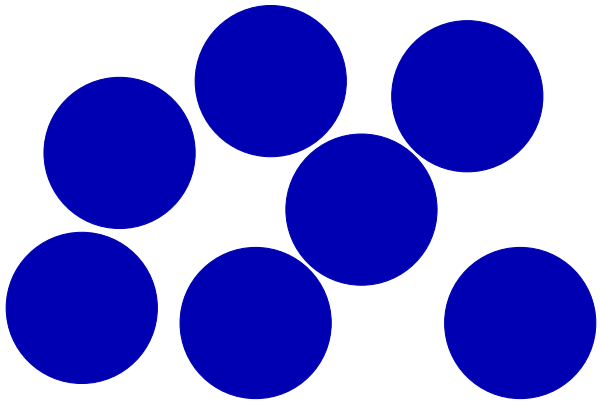

Figure 1.2 Arrangement of atoms in an amorphous material

X-Ray diffraction (XRD) utilizes x-rays to non-destructively probe the inner atomic layers of materials[1]. In this work it is used to probe different depths of doped silicon to see dopant levels as a function of depth. As the x-ray interacts with the sample it will reflect, refract, and diffract. Diffraction is the process of note for XRD, and the only one that will be investigated for this work.

The XRD that will be utilized is a PANalytical Aeris[2] with tension set at 40kV, current at 15mA. The optics include a beta nickel filter, 0.04 soller slits, 13mm beam mask, 0.28° parallel plate collimator, and the detector set in 0D mode. The beta nickel filter filters out unwanted wavelengths that are produced; this helps with Bragg's law (eq 1.1). The soller slits control the beam width as well as the beam mask; the 13mm beam mask controls the width of the beam in order to irradiate only the sample. The parallel plate collimator selects only the diffracting x-rays that correspond to the current theta angle, as well as only allowing for parallel x-rays. The 0D mode sums up all the photons that interact with it at the specific angle at which the detector is currently positioned. A variety of divergence slits were chosen depending on the incident angle as divergence slits control irradiated length.

When XRD is used on crystalline solids, a diffraction pattern will emerge. This

diffraction pattern arises from Bragg's law:

$$2d\sin\theta = n\lambda \tag{1.1}$$

Where λ is the wavelength of the light, and d is the slit spacing, which are the different atomic planes within the sample. The planes are interatomic spacings of non-neighboring atoms as well, instead of only to the nearest neighbors. These planes of atoms then act as a diffraction grating for the incident light, causing constructive and destructive interference with all other planes (see figure 1.3). All of these in superposition produce a graph that shows sharp peaks correlating directly to the atomic plane's spacing (shown in figure 1.4). Since the depth of the doping is the focus of this work, single crystal XRD was used. Single crystal XRD leaves the sample intact, with the plane of atoms aligned in their preferred orientation[1] in order to see the correct diffraction pattern (see figure 1.5). This is in contrast to powder diffraction, which first pulverizes the sample into a powder in order to achieve a homogenous mix of all constituents in the sample. Due to the powderization, preferred orientation becomes meaningless since all orientations are now present.

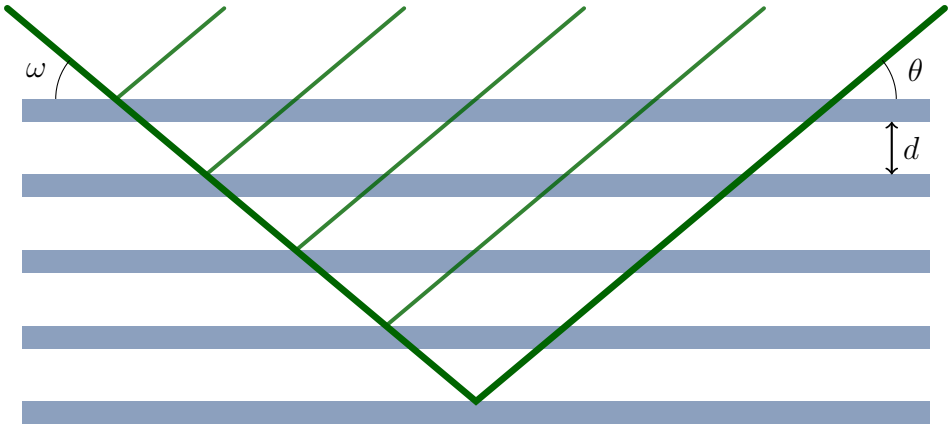

Figure 1.3 Representation of diffraction from the atomic planes

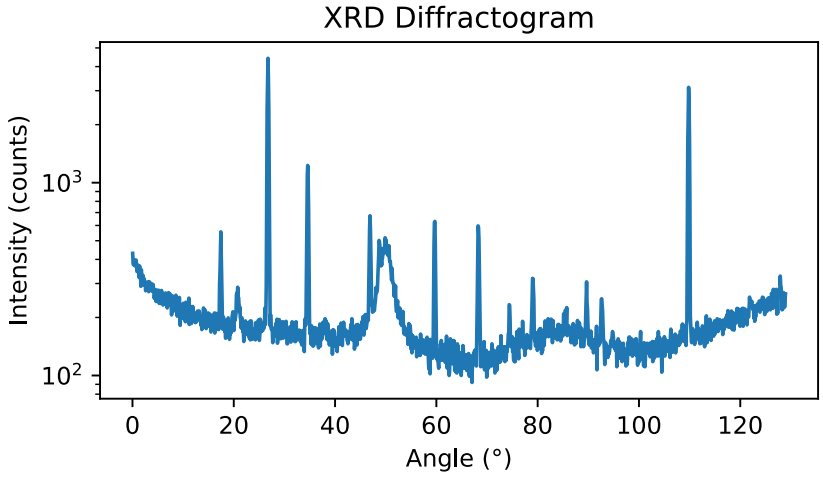

Figure 1.4 Diffractogram of a single crystal crystalline solid

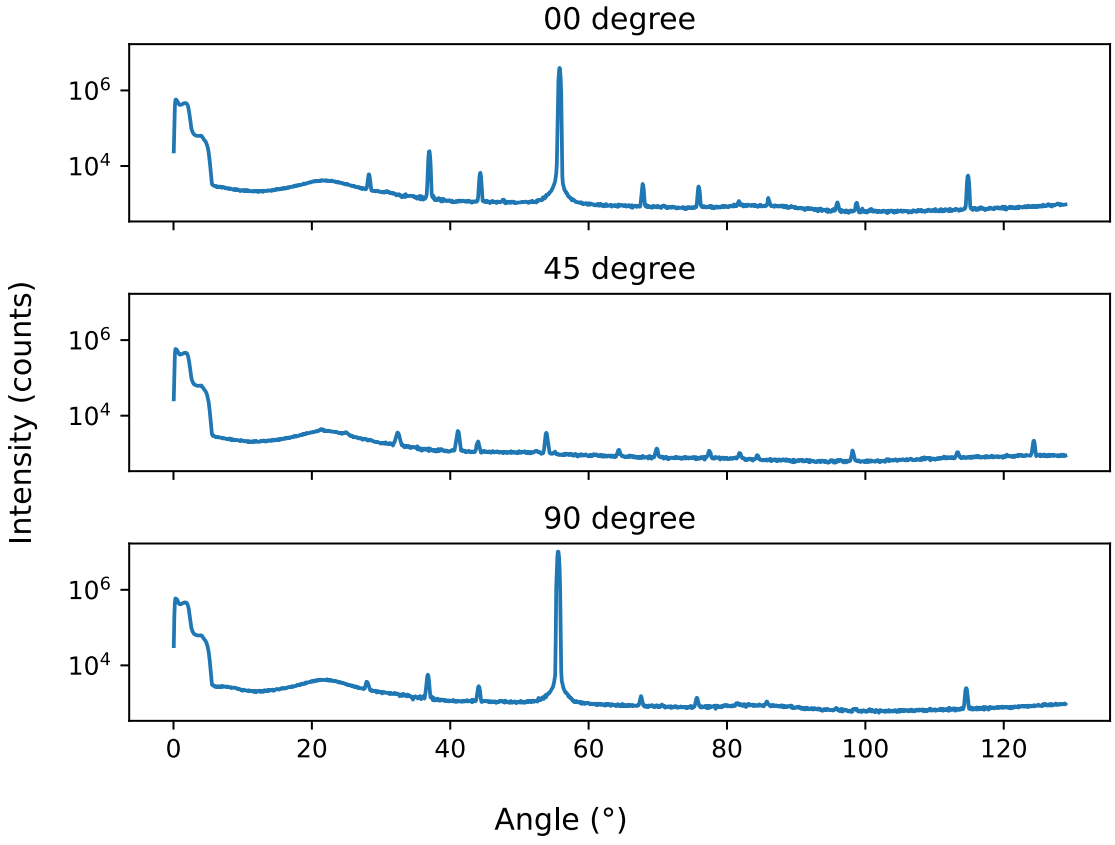

Figure 1.5 Comparison of preferred orientation with 45° and 90° off preferred orientation

Amorphous solids under the x-ray beam behave in a similar manner. The difference being because every atom is arranged randomly, there are an infinite number of planes all with their own spacing. As shown in figure 1.6, this correlates to a moderately low angle hump (called an amorphous hump) with all spacings that would correlate to higher angled peaks being nonexistent because of destructive interference[3–5].

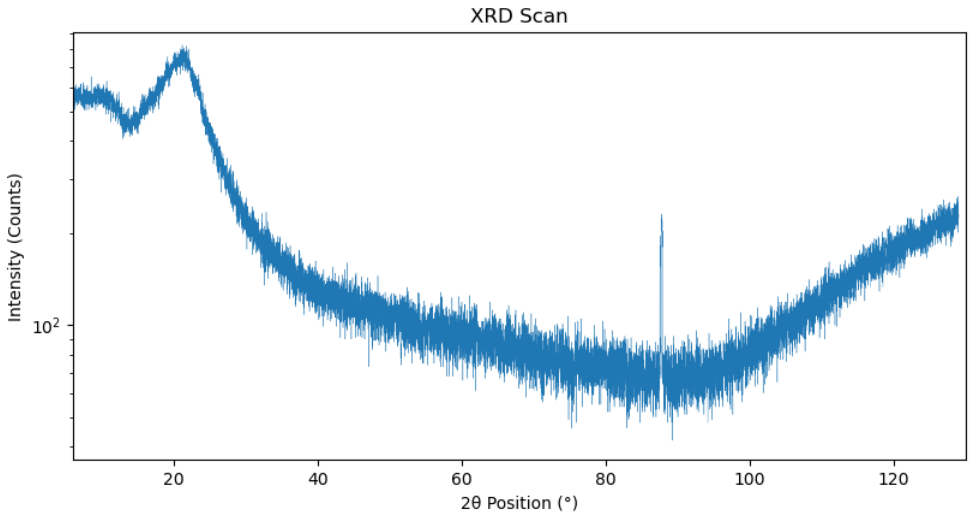

Figure 1.6 Diffractogram of amorphous solid (the peak near 88° is from the sample holder)

Doping is adding another substance (called a dopant) to a material (called a substrate) to change electrical properties of that material. This increases the desirability of the material in future applications in which it will be used. The materials analyzed in this work are silicon doped with phosphorous, silicon doped with boron, and silicon. The first two materials will be best thought of as a gradient from pure phosphorous, or boron, to pure silicon from top to bottom. Silicon is a crystalline material, while phosphorous and boron are the amorphous part in the samples analyzed in this work. This means that the diffractogram will be a superposition of an amorphous diffractogram on a crystalline diffractogram. The silicon sample was only used to verify

that the amorphous hump was present on the diffractograms. These materials were given by the Semiconductor group at Brigham Young University-Idaho, and chosen to assist the group. The processes developed will be used to assist the Surface Physics group in characterization of future metal deposition.

Chapter 2

Methods

The process by which the XRD is used in this work to probe increasingly deeper depths is called grazing incidence x-ray diffraction[1] (GIXRD; also called glancing incidence x-ray diffraction[6]). GIXRD holds an incident angle relative to the surface of the sample (called omega (ω)), while the detector on the diffracted beam side sweeps over a range of angles (figure 2.1). The detector is used in 0D mode in conjunction with a parallel plate collimator; this means it simply counts all the x-rays that interact with it. The counts get added to bins corresponding to the current detector angle according to this equation: $2(\omega + \theta)$, with θ being the current detector angle. After the detector has swept through all programed angles, a new scan is started with a different ω corresponding to a different depth.

The different incident angles probe different depths due to the different path lengths they provide the x-rays as they interact with the samples. This is due to the exponential attenuation of intensity as the beam travels; given by the equation:

$$I(y) = I_0 e^{-\alpha y} \tag{2.1}$$

with $\alpha = 2\omega n_I / c$[7, 8]. With the complex index of refraction (n_I) strongly dependent on the incoming wavelength. The x-ray source is copper, producing K_α in

abundance with some K_β. Since one wavelength provides the most uniformity on the diffractogram, the incident beam optics include a filter to limit the unnecessary wavelengths. K_α is what is most common, so the K_β gets mostly filtered out by a nickel filter. This results in a x-ray beam that has a wavelength of 1.54Å. It is these subtle differences that allow for the determination of different ratios of dopant to substrate.

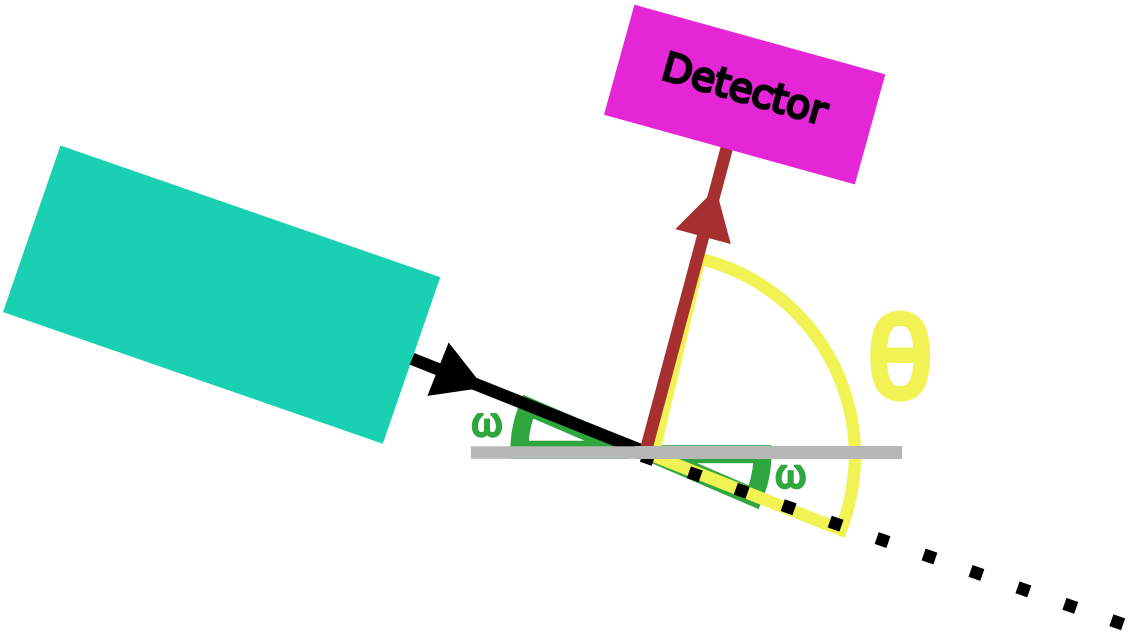

Figure 2.1 Diagram of XRD utilizing GIXRD

Three different methods for determining relative percentages of the dopant in the substrate are used. The methods are: 1. Intensity[1], 2. Curve Fitting, and 3. Summation. Before discussing the methods used to analyze the sample, it is important to know what assumptions were made. The first of these assumptions is that the mixture of the probed depth is uniform. The next assumption is from the exponential nature of attenuation; it is that the intensity of the x-ray has been attenuated by 90%. Then thirdly, that the sample is put in its preferred orientation that allows for the silicon structure to be aligned with the x-ray beam. The last assumption is that the index of refraction is the same as bulk samples[6] as those

values will be utilized.

Method 1: Intensity

This method takes the highest intensity count from the amorphous hump, and the highest intensity count from the crystalline peaks as input parameters, and calculates the ratio of them. This ratio is then the relative percentages of the dopant and substrate[1]. The following formula is used for the calculation:

$$m = \frac{I_a}{I_a + I_c} \tag{2.2}$$

Where I_a is the highest count of the amorphous hump, I_c is the highest count of the crystalline peaks, and m is the mixture percent.

Method 2: Curve Fitting

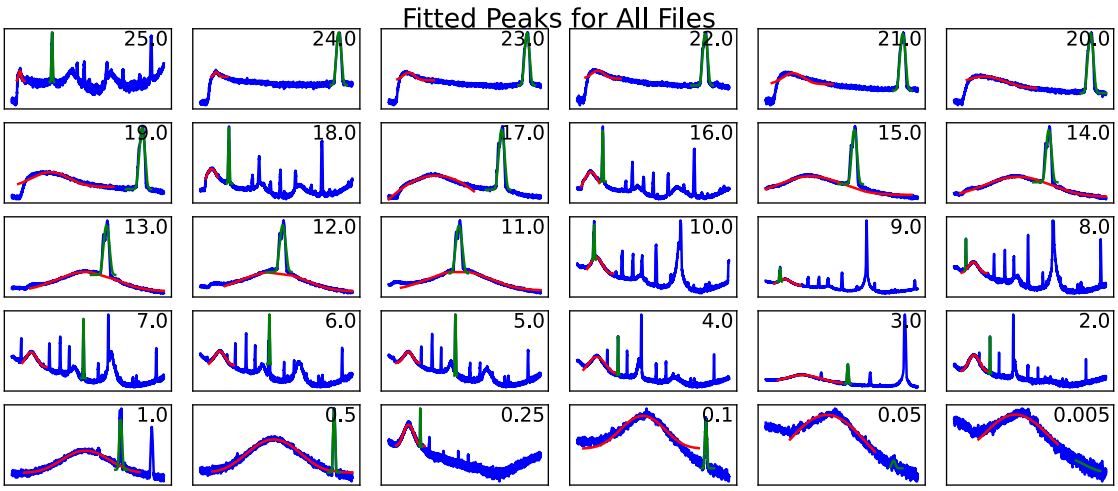

Figure 2.2 Diffractogram with relevant peaks fitted, and incident angle shown

The amorphous hump, and the crystalline peaks can be approximated by Gaussian curves. As such, it is possible to fit a curve to the hump, and the desired peak, as

well as a background baseline. With this fit, analytic integration is performed. The values from the integrations are then taken as a ratio as in the intensity method. This method also allows for the background baseline to be subtracted out.

Method 3: Summation

This method is similar to the curve fitting method, but instead of fitting the hump and peak to a Gaussian, a numerical integration is performed directly on the data. This was implemented to compare to the curve fit method due to mismatches in some of the fits and their peaks (see figure 2.2). This numerical integration sums up the heights in the region of the relevant area to take their ratio. As stated, only the heights are summed; this is due to the spacing between all points being identical. The mixture percentage is derived as follows:

$$
\begin{aligned}
m &= \frac{\sum_{\theta_i}^{\theta_f} y_a dx_a}{\sum_{\theta_i}^{\theta_f} y_a dx_a + \sum_{\theta_i}^{\theta_f} y_c dx_c} \\
dx_a &= dx_c = Constant \\
m &= \frac{dx_a \sum_{\theta_i}^{\theta_f} y_a}{dx_a \sum_{\theta_i}^{\theta_f} y_a + dx_c \sum_{\theta_i}^{\theta_f} y_c} \\
m &= \frac{dx_a \sum_{\theta_i}^{\theta_f} y_a}{dx_a \left(\sum_{\theta_i}^{\theta_f} y_a + \sum_{\theta_i}^{\theta_f} y_c \right)} \\
m &= \frac{\sum_{\theta_i}^{\theta_f} y_a}{\sum_{\theta_i}^{\theta_f} y_a + \sum_{\theta_i}^{\theta_f} y_c}
\end{aligned}
\tag{2.3}
$$

Where y_a, and y_c are the counts of the current θ position for the amorphous and crystalline parts respectively. With dx_a, and dx_c as the spacing between the θ positions for the amorphous and crystalline parts respectively. The quantity m is the mixture amount, and θ_f, and θ_i are the starting and ending θ positions for the amorphous hump or crystalline peak respectively. This method was developed as a comparison to the curve fit method as some fits are not ideal (as figure 2.2 shows).

Chapter 3

Analysis

After getting the diffractogram the ranges for the amorphous hump, and most intense crystalline peak were taken as input in a text file. This text file was then read by the python program (linked in appendix B) developed to determine composition, and depth. The composition was determined by the methods in the previous chapter. The depth was determined by mixing the indices of refraction of the materials in the sample (phosphorous and silicon) using the composition percent as the weights. Indices of refraction were used from The Center For X-Ray Optics (linked here)[9]. The above was combined by using the following equation:

$$n = m_a n_a + m_c n_c \tag{3.1}$$

Where n is the layer's index of refraction, n_a and n_c are the index of refraction for phosphorous and silicon respectively. The quantities m_a and m_c are the mixture fraction of the phosphorous and silicon respectively.

This new index of refraction for the layer was then converted into an attenuation coefficient by the following:

$$\alpha = \frac{4\pi n_I}{\lambda} \tag{3.2}$$

Where n_I is the imaginary component of the layer's index of refraction, and λ is the wavelength[8]. The inverse of the attenuation coefficient is then the skin depth of the material, or the depth at which the x-rays have attenuated to a third of the original intensity. This skin depth was then applied until 90% attenuation was achieved. The vertical component of the path length was then taken to be depth from the surface of the material (as shown below in figure 3.1).

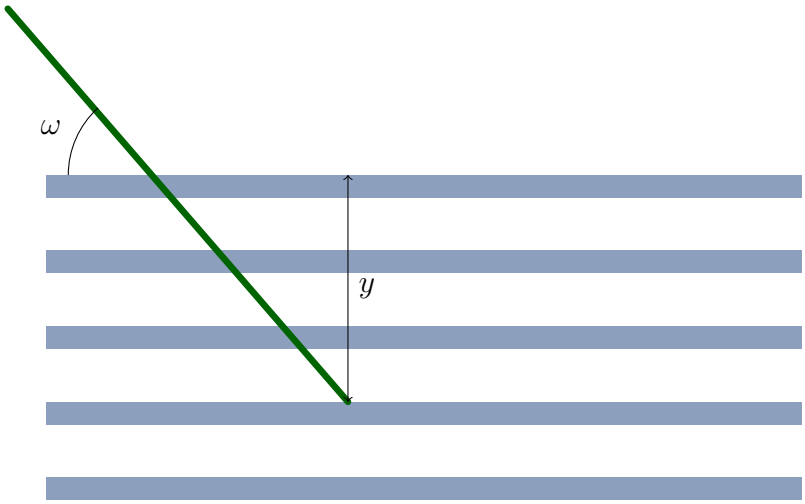

Figure 3.1 Path length to depth into the sample

Results from the methods are given in the figure below:

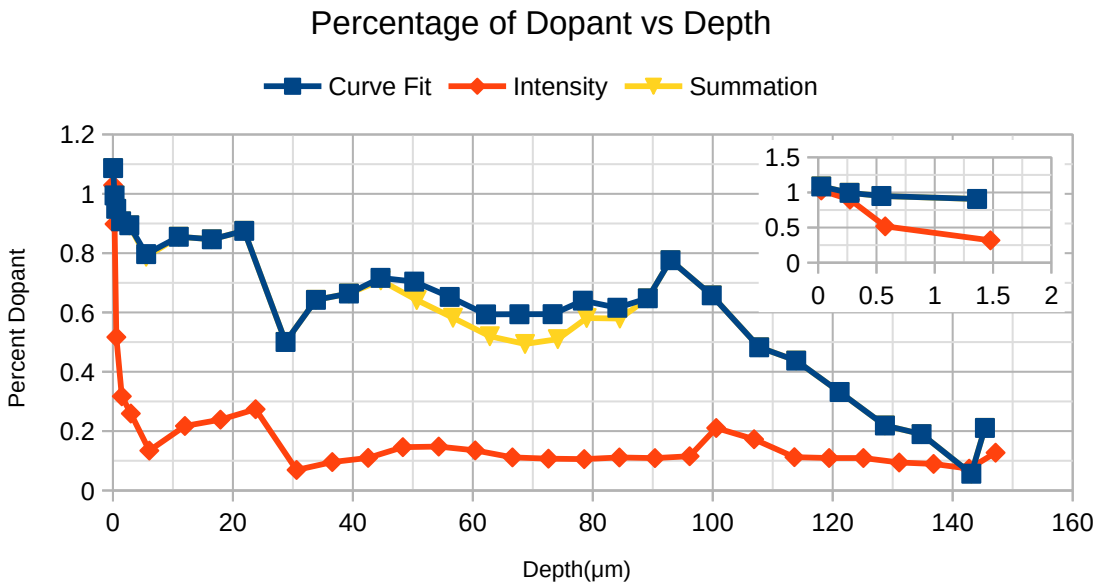

Figure 3.2 Percentage of amorphous vs depth for the three methods

From figure, 3.2 we can see that the intensity method is not in agreement with the curve fit or summation methods. The curve fit and summation methods are expected to be in agreement with each other since the methods are both integral methods. It should be noted that the three methods seem to give a value greater than unity for the lowest depth, but this is an artifact of forcing the program to find data that is not there. At the omega angle that corresponds to this low depth, the crystalline peaks do not appear. This means only an amorphous hump is available for the data analysis.

Chapter 4

Conclusion

Using GIXRD to determine relative composition of samples led to the development of three analysis methods; intensity, curve fit, and summation. The curve fit and summation methods utilized integration, and their results are more closely aligned. The intensity method uses peak intensity ratios, and provides results that noticeably differ. All three methods provide reasonable agreement as to the depth that each incident angle probed.

Due to the time constraints of the project, future work will be needed to discriminate the methods further to determine their effectiveness. The Surface Physics team has been manufacturing a magnetron deposition machine which will be used to create bilayers of metal. As part of the equipment that will be used to produce these bilayers is a quartz oscillator that will change frequency as metal gets deposited onto it. This data can then be compared to the analysis methods contained herein to determine their correlation. Future work will also be needed to introduce nonuniform layers to the methods. Preliminary work has been pursued, but much more time will be needed to get it fully integrated into the methods. There were also some anomalies that were present in the diffractograms that were unable to be correlated to anything

found in the literature. Figuring out what these anomalies mean could lead to more information gained from the diffractograms.

Bibliography

[1] A. Pandey, S. Dalal, S. Dutta, and A. Dixit, "Structural characterization of polycrystalline thin films by X-ray diffraction techniques," Journal of Materials Science: Materials in Electronics **32,** 1341–1368 (2021).

[2] M. Panalytical, *Aeris User Guide*.

[3] G. L. Parks, M. L. Pease, A. W. Burns, K. A. Layman, M. E. Bussell, X. Wang, J. Hanson, and J. A. Rodriguez, "Characterization and hydrodesulfurization properties of catalysts derived from amorphous metal-boron materials," Journal of Catalysis **246,** 277–292 (2007).

[4] C. Achilles *et al.*, "AMORPHOUS PHASE CHARACTERIZATION THROUGH X-RAY DIFFRACTION PROFILE MODELING: IMPLICATIONS FOR AMORPHOUS PHASES IN GALE CRATER ROCKS AND SOILS.," In *49th Lunar and Planetary Science Conference 2018 (LPI Contrib. No. 2083)*, 2083 (2018).

[5] A. van Riessen, E. Jamieson, H. Gildenhuys, R. Skane, and J. Allery, "Using XRD to Assess the Strength of Fly-Ash- and Metakaolin-Based Geopolymers," Materials 18 (2025).

[6] P. Colombi, P. Zanola, E. Bontempi, and L. E. Depero, "Modeling of glancing incidence X-ray for depth profiling of thin layers," Spectrochimica Acta Part B: Atomic Spectroscopy **62,** 554–557 (2007), a Collection of Papers Presented at the 18th International Congress on X-Ray Optics and Microanalysis (ICXOM 2005).

[7] J. Liu, R. E. Saw, and Y.-H. Kiang, "Calculation of effective penetration depth in X-ray diffraction for pharmaceutical solids," Journal of Pharmaceutical Sciences **99,** 3807–3814 (2010).

[8] E. Hecht, *Optics*, 4th intern ed. (Addison Wesley, 2002).

[9] B. L. Henke, E. M. Gullikson, and J. C. Davis, "X-ray interactions: photoabsorption, scattering, transmission, and reflection at E=50-30000 eV, Z=1-92," Atomic Data and Nuclear Data Tables **54,** 181–342 (1993).

Appendix A

Percent Dopant Data

The following is data for the intensity and summation methods, with their fractional uncertainties.

omega	Intensity	Intensity Fractional Uncertainty	Summation	Summation Fractional Uncertainty
0.005	1.0291		1.0869	
0.05	0.8983	0.0110	0.9946	0.0001
0.1	0.5168	0.0239	0.9495	0.0003
0.25	0.3174	0.0263	0.9070	0.0004
0.5	0.2593	0.0313	0.8936	0.0004
1	0.1344	0.0389	0.7877	0.0008
2	0.2172	0.0197	0.8552	0.0003
3	0.2387	0.0146	0.8467	0.0002
4	0.2737	0.0142	0.8752	0.0002
5	0.0690	0.0181	0.5004	0.0005
6	0.0958	0.0179	0.6426	0.0004
7	0.1098	0.0183	0.6639	0.0004
8	0.1459	0.0203	0.7082	0.0004
9	0.1478	0.0138	0.6417	0.0003
10	0.1351	0.0142	0.5820	0.0004
11	0.1115	0.0157	0.5196	0.0004
12	0.1071	0.0165	0.4938	0.0005
13	0.1056	0.0169	0.5099	0.0005
14	0.1113	0.0173	0.5812	0.0004
15	0.1091	0.0185	0.5794	0.0004
16	0.1153	0.0122	0.6478	0.0003
17	0.2106	0.0136	0.7765	0.0002
18	0.1726	0.0131	0.6580	0.0003
19	0.1123	0.0249	0.4827	0.0008
20	0.1093	0.0273	0.4377	0.0009
21	0.1093	0.0292	0.3320	0.0014
22	0.0942	0.0341	0.2191	0.0021
23	0.0894	0.0364	0.1900	0.0024
24	0.0735	0.0427	0.0564	0.0053
25	0.1273	0.0333	0.2107	0.0025

Figure A.1 Table for percentage of amorphous vs omega for the three methods with fractional uncertainty

Appendix B

Data and Code used

The following link is where the data and code is stored online:

https://github.com/MarkS5001/Senior-Research-Spring-2025-/tree/main